Surface alloy formation and the structure of $c(2 \times 2)$-Sn/Ni(100) determined by low-energy alkali-ion scattering

Y. D. Li, L. Q. Jiang, and B. E. Koel

Department of Chemistry, University of Southern California, Los Angeles, California 90089-0482

(Received 7 May 1993)

The growth of Sn on Ni(100) and the structure of the $c(2 \times 2)$-Sn/Ni(100) surface were studied using 500-eV Li^+ scattering, Auger-electron spectroscopy, and low-energy electron diffraction (LEED). The polar-angle dependence of the Li^+ scattering from Sn and Ni of the $c(2 \times 2)$-Sn/Ni(100) bimetallic surface prepared at 250 K reveals that an ordered two-dimensional surface alloy is formed. However, Sn is not coplanar with the first Ni layer, but buckled above the Ni plane by 0.44 ± 0.05 Å. These studies show that Sn and Ni mixing occurs at low temperatures. When the surface alloy prepared at 250 K was annealed to above 400 K, additional features appeared in the polar-angle dependence of Li^+-Ni single scattering, suggesting that small surface reconstructions occur on the $c(2 \times 2)$ alloy surface. Further annealing to 900 K results in a LEED pattern characterized by a splitting of the half-order beams into quartets. Formation of out-of-phase domains may be responsible for this LEED pattern.

I. INTRODUCTION

The growth of metals on metals in a controlled manner provides tremendous opportunities for preparing ordered surface alloys, overlayers, and superlattices for desired catalytic, noncorrosive, and magnetic properties.[1,2] Many studies of metal deposition have been concerned with the growth and structure of overlayers. But recently, more and more systems have been explored which show the formation of ordered surface alloys.[3-8] The bimetallic surfaces prepared by this approach have unique reactivity which leads to considerable insight into the molecular details of how adsorbates bond and react at these surfaces.[9-11] Surface alloy formation is characterized by the intermixing of two metal components on the topmost atomic plane. Usually alloy formation is expected if the constituent metals have similar metallic sizes and tend to form miscible solutions over a wide range of compositions. If the constituents have dissimilar size but tend to form intermetallic compounds (e.g., Sn-Ni or Sn-Pt), then one can see a nucleated intermetallic phase formed on the surface.

Bimetallic catalysts involving Sn and late transition metals are useful industrial catalysts for various hydrocarbon reactions. Alloy surfaces may play a role in this chemistry and are certainly important to study. The possibility that Sn and Pt formed a surface alloy was first proposed by Paffett and Windham when they studied the Sn/Pt(111) system.[5] Recently, systematic studies of Sn on the (111) surfaces of Ni, Cu, and Pt have been conducted by Overbury and co-workers,[6-8] using low-energy alkali-ion scattering. The common surface alloy made with all these substrates has a $p(\sqrt{3} \times \sqrt{3})$-$R \, 30°$ low-energy electron-diffraction pattern, and is formed predominantly upon annealing. Because of the size mismatch between Sn and substrate atoms (the atomic diameters of Sn, Ni, Cu, and Pt are 2.81, 2.49, 2.56 and 2.77 Å, respectively), Sn atoms tend to buckle outward by an amount which is linearly related to the substrate lattice constant, indicating that rippling provides lateral strain relief within the layer. Two important questions still remain unanswered. First, would Sn form surface alloys with surfaces other than (111)? Second, if so, how does the magnitude of the surface rippling depend upon first-layer versus second-layer coordination? To shine some light on these questions, we picked the Sn/Ni(100) system as our first case study. Although the systems of Sn/Ni(100) (Ref. 12) and Sn/Pt(100) (Ref. 11) have been studied previously, the structures of these surfaces were not determined. Paffett *et al.*[11] conjectured that the $c(2 \times 2)$ pattern arose from an ordered SnPt surface alloy for the Sn/Pt(100) system. It was not possible in those studies to distinguish between Sn adatoms and Sn incorporated into the top layer to form an alloy. Also, if alloys were formed, it certainly was not known whether the alloyed surface was planar or corrugated.

We report here, to our knowledge, the first determination of the surface structure of Sn on Ni(100). In contrast to Sn/Ni(111) or other (111) faces studied before,[7] a very clear $c(2 \times 2)$ LEED pattern for a Sn coverage of 0.5 ML (monolayer) is observed even at deposition temperatures as low as 250 K. This LEED pattern is retained when the sample is annealed up to 800 K. Our results show that this $c(2 \times 2)$-Sn/Ni(100) structure is a surface-alloy phase, and that the amount of outward buckling of Sn atoms is very similar to that for the Sn/Ni(111) system.

II. EXPERIMENTAL METHODS

The experiments were carried out in a two-level UHV system which was briefly described before.[13] The base pressure of the chamber is 8×10^{-11} Torr, and the typical operating pressure is $1-2 \times 10^{-10}$ Torr. The upper level contains a four-grid LEED optics, which is also used with a grazing incident electron gun for Auger-electron spectroscopy (AES) measurements. The lower level contains a Colutron ion gun which provides collimated and monoenergetic ion beams ($\Delta E/E = 0.25\%$) to the chamber. The cross section of the ion beam is formed by a 1.6-mm-diam aperture, and the typical beam current

density used in our experiment is 15–25 pA/mm². The chamber is equipped with two spherical sector electrostatic analyzers (ESA's) for analyzing scattered ions. One ESA (from the COMSTOCK Co., mean diameter = 73 mm) is rotatable, allowing variation of the total laboratory scattering angle, θ, from 0° to 163°. The other ESA (Perkin-Elmer, mean diameter 279.4 mm) is fixed at a scattering angle of 144°, and is equipped with a MCD (multichannel detector) comprised of dual multichannel plates configured to act as 16 discrete detectors. The availability of the small rotatable ESA allows us to measure the scattering-angle dependence of critical angles in order to determine scattering potentials and also to check the origin (e.g., single or multiple scattering) of peaks in the energy spectrum. Both the polar angle of incidence ψ (measured from the plane of the sample surface as determined by laser alignment) and azimuthal angle of incidence Φ (measured from the [110] azimuth as determined initially from LEED alignment and then finely adjusted according to azimuthal scans) are driven by stepping motors which are interfaced to and controlled by a computer. The accuracy of ψ, Φ, and θ are ±0.5°, ±1°, and ±0.5°, respectively.

The availability of two analyzers also provides a means to calibrate the polar incident angle. We put the two ESA's on either side of the incoming ion beam with mirror-symmetric scattering geometries (scattering angle 144°), and align the clean Ni(100) substrate along one particular azimuth, say [110]. After taking the polar incident-angle scan using one ESA, the sample is rotated by 180° and a similar polar incident-angle scan is taken using the other ESA. If our sample polar alignment is perfect then these two polar incident-angle scans are exactly the same, otherwise there will be a shift in the position of the peaks. Based on this shift the polar-angle misalignment along this particular azimuth can be estimated. With this internal calibration procedure, one

can constantly check our polar-angle accuracy during the whole experiment. We believe that this calibration results in a polar-angle accuracy of better than 0.5°.

The 10-mm diameter, 1-mm-thick Ni(100) crystal was held onto the sample stage by two 0.38-mm Ta wires. The sample could be heated resistively to 1200 K, or cooled to 210 K by flowing liquid nitrogen through the sample stage. This cooling capability turned out to be very important for this experiment. The crystal was cleaned by repeated cycles of sputtering with the sample hot (1010 K), and subsequent annealing in vacuum to 1030 K. Oxygen exposures were also used to remove residual carbon from the surface.

The Sn doser was constructed from 0.13-mm Ta foil, making an enclosed boat with a small pin-hole in the top. A 6-N-purity Sn ingot was placed in this crucible oven and was thoroughly outgassed. By passing a current of 9 A through two small Ta wires suspending the oven, Sn was deposited at a rate of about 0.04 ML/min with a background pressure below 2×10^{-10} Torr.

III. RESULTS

A. Characterization of Sn deposition on Ni(100) by AES and LEED

The Ni AES peak-to-peak amplitude versus Sn deposition time (Auger uptake plot) is shown in Fig. 1 for the growth of Sn on Ni(100) at 250 K. The inset shows the corresponding Sn AES uptake plot. Two breaks denoted as A and B can be seen clearly in the Ni AES signals. This is very similar to the results reported previously by Oda and Rhead.[12] They assigned the break at B to the formation of a dense Sn monolayer, based on the attenuation of the Ni signal, while ascribing the break at A to a sudden change in sticking probability that might be correlated with a change of adsorbate structure. We observed the best $c(2\times2)$ LEED pattern in terms of sharpness and contrast at or near the break at A, and the patterns became progressively worse at higher Sn deposition times. This "best" $c(2\times2)$ pattern actually could be made even sharper once the surface was annealed to 500–800 K, and both the Sn and Ni AES intensities remained almost the same as those at 250 K. It seems reasonable therefore to assign the first break at A to one-half-monolayer coverage. A similar AES uptake curve was found in the $c(2\times2)$-Pd/Cu(100) system,[4] and these authors also interpreted the first change of slope as due to the completion of a $c(2\times2)$ mixed layer. It is unusual to have a break in this type of plot at half-monolayer coverage, but one of the possible explanations is that this break relates to the finishing of surface-alloy formation. As will be shown below, our angle-resolved alkali-ion scattering spectroscope (ALISS) results clearly show the ordered $c(2\times2)$ structure is a surface-alloy phase.

The $c(2\times2)$ is not the only LEED pattern observed. Once the $c(2\times2)$-Sn/Ni(100) surface was annealed to 900 K, we observed a complex LEED pattern with each $(\frac{1}{2},\frac{1}{2})$ beam clearly split into a quartet. Annealing to this temperature causes a decrease in the Sn AES signal, probably due to diffusion of Sn into the bulk of the crys-
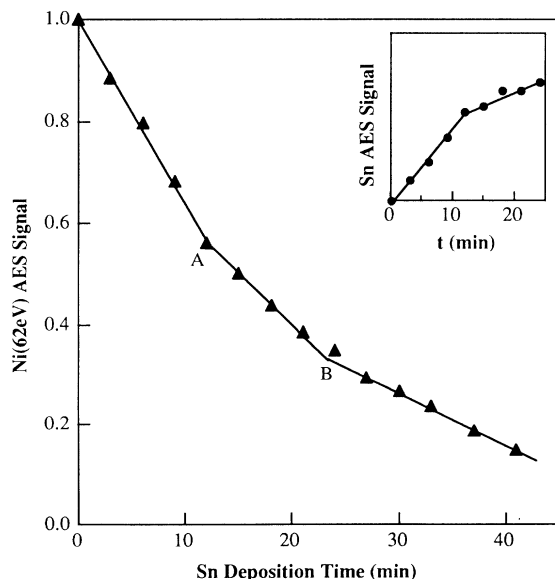

FIG. 1. The Ni (62-eV) peak-to-peak intensity (normalized to the bulk Ni AES signal) vs the deposition time of Sn on Ni(100) at 250 K. The inset shows the corresponding Sn AES intensity (arb. units).

tal. This kind of LEED pattern has been observed for the adsorption of nitrogen on W(100),[14,15] and was explained as the formation of (4×4) nitrogen adatom domains with antiphase boundaries between them. We will discuss this more complicated surface structure in Sec. III D.

B. Determination of the TFM scattering potential

The scattering potential for the interaction of probing ions and surface atoms must be known in order to apply low-energy ion scattering to the analysis of surface structure. The Molière approximation to the Thomas-Fermi potential (TFM potential) is widely used with the binary collision approximation.[16] An adjustable parameter in this potential, C, has to be determined before it can be applied to a real structure determination. One way of obtaining the C parameter is to calculate the critical angle ψ_c as a function of the laboratory scattering angle θ, and compare it to the experimental data (usually with ψ_c taken at 90% of maximum intensity). This $\psi_c(\theta)$ dependence originates from the fact that the distance of closest approach between the projectile and the target atom is a function of the incidence angle when the incident beam aligns along a chain of atoms. This approach was first suggested by Overbury.[16] It is not only an effective way
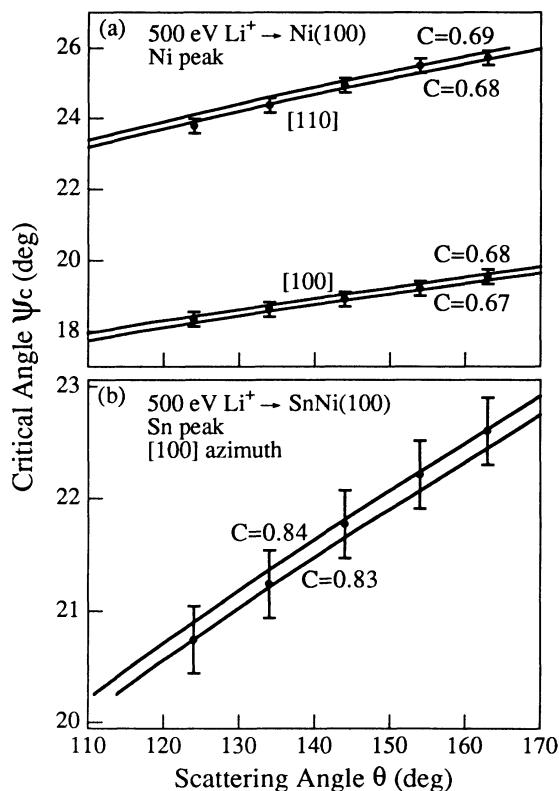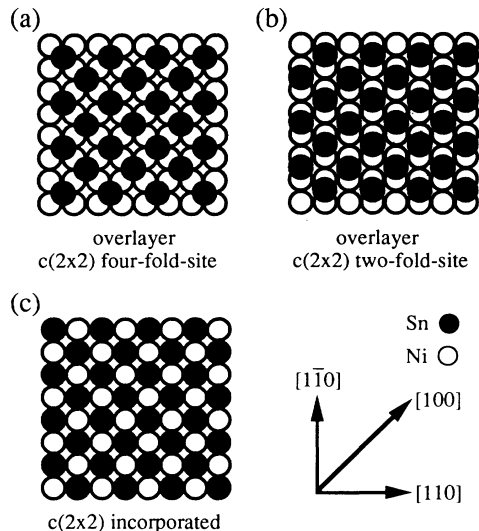

FIG. 3. Three proposed models for the $c(2\times2)$-Sn/Ni(100) structure: (a) Overlayer $c(2\times2)$ structure with Sn atoms sitting at fourfold sites; (b) overlayer $c(2\times2)$ structure with Sn atoms sitting at twofold bridge sites; and (c) incorporated $c(2\times2)$ structure with Sn atoms replacing first-layer Ni atoms.

FIG. 2. Plots of critical angles ψ_c as a function of laboratory scattering angle θ. Measured critical angles (points) are compared with theoretically calculated critical angles (solid curves) for a TFM potential with various values of the screening length C. Error bars shown for the measured angles are based on multiple measurements. (a) Li$^+\to$Ni single scattering on the clean Ni(100) surface along both [110] and [100] azimuths. (b) Li$^+\to$Sn single scattering on the $c(2\times2)$-Sn/Ni(100) surface along the [100] azimuth.

to decide the C parameter, but also a self-calibration procedure. Based on the known interatomic spacings along one given azimuth, we are able to determine the scattering potential for Li$^+$ interacting with Ni and Sn.

The value of C for the Li$^+\to$Ni potential was determined by scattering 500-eV Li$^+$ from clean Ni(100) along both [110] and [100] azimuths. Figure 2 shows the calculated and measured dependences of the critical angle ψ_c on the laboratory scattering angle θ. To compare with Overbury's study of Sn/Ni(111),[8] ψ_c is determined after the scattered ion intensity detected at each polar angle ψ is multiplied by sin(ψ) (we will refer to this procedure as a "sine correction" throughout this paper). The theoretical critical angle was calculated using the MARLOWE simulation package considering only chainlike scattering.[16] Data from both [110] and [100] azimuths consistently indicate $C_{\text{Ni}}=0.68\pm0.02$, which agrees well with a previously determined value of 0.68.[8]

The value of C for the Li$^+$-Sn potential was determined from the cold-deposited (<250 K) $c(2\times2)$-Sn/Ni(100) surface along the [100] azimuth. For all of the proposed models shown in Fig. 3, which will be discussed below, the Sn atoms form a single chain in the [100] direction with a spacing of 3.52 Å. This known interatomic spacing allows us to apply the same method outlined above to obtain C_{Sn}. A sine correction is also made for this determination of ψ_c. As shown in Fig. 2(b), C_{Sn} is determined to be 0.84±0.03. This value is lower than $C_{\text{Sn}}=0.90$ obtained from the $p(\sqrt{3}\times\sqrt{3})$-$R\,30°$-Sn/Ni(111) surface.[8]

C. Structure determination
of cold-deposited $c(2\times2)$-Sn/Ni(100)

Based on the $c(2\times2)$ LEED pattern, three likely structural models were proposed as shown in Fig. 3.

Other models conceivably exist but involve extensive distortions of the Ni lattice and, therefore, are not considered at this time. Sn adatoms sit in fourfold hollows and twofold bridge sites for the two proposed overlayer models in Fig. 3(a) and 3(b), respectively. Although we have no direct evidence for placing the Sn atoms in these specific sites, the most chemically and physically consistent picture of surface bonding is to maximize Sn surface-atom coordination. The $c(2\times2)$ substitutional model in Fig. 3(c) is derived from one-half monolayer of Sn atoms replacing the first-layer Ni atoms. Angle-resolved ALISS can distinguish between these models and allow for the elucidation of the correct surface structure.

In this section, we present results for cold-deposited (at 250 K) $c(2\times2)$-Sn/Ni(100). The energy distribution of Li^+-ion scattering for this surface is shown in Fig. 4. Since the Sn single scattering peak ($E/E_0 = 0.78$) is fully separated from the Ni single scattering peak ($E/E_0 = 0.63$), the Sn polar-angle scans (analyzer fixed at $E/E_0 = 0.78$ and varying the incident angle) are unlikely to be greatly affected by the inelastic background. The scattering peak positions in Fig. 4 might depend on the polar angle, and this was studied by taking a series of energy scans along the [100] azimuth at different polar angles (from 15° to 90°). The results show that the Ni or Sn peak was shifted by about 2 eV within this angle range, and that in the same angle range the full width at half maximum (FWHM) of both peaks was 15±3 eV. By setting the large ESA pass energy at 187 eV, the configuration of the 16-channel MCD allowed us to integrate the intensity within the peak region of $E_{peak}\pm12$ eV. This peak region almost covered the whole peak, and thus the influence of the peak shift during the polar-angle scan is minimized.

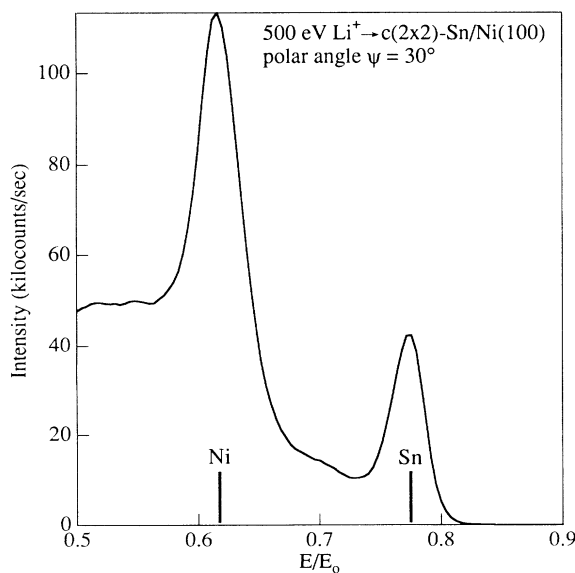Figure 5 shows the effects of Sn deposition upon the polar-angle scans for 500-eV Li^+ scattering from Ni. Notations such as $S_{Ni\text{-}Ni}$ are used to label specific peaks, and $S_{Ni\text{-}Ni}$ means that peak is produced by Ni-atom shadowing effects on the neighboring Ni atom along a specified azimuth. Compared with the polar-angle scans from the clean Ni substate, two main features were observed: (i) along the [100] azimuth, we could not distinguish any pronounced differences between the clean and Sn-covered Ni(100) surface; and (ii) along the [110] and its equivalent [1$\bar{1}$0] azimuth, the $S_{Ni\text{-}Ni}$ peak was diminished and a peak labeled $S_{Sn\text{-}Ni}$ appeared at about $\psi=41°$. Based on these observations, we can clearly determine the correct structure from the proposed models shown in Fig. 3. If the $c(2\times2)$ structure with Sn adatoms occupying fourfold sites was correct, we should see a shadowing peak along [100] formed by Sn atoms shadowing the neighboring Ni atoms. Second, along the [110] or [1$\bar{1}$0] azimuth, we should see similar incident angle scans for clean Ni(100) and Sn/Ni(100). Obviously these predictions are contrary to what we have observed along these azimuths, and so we can easily exclude the $c(2\times2)$ fourfold-site overlayer model. As for the $c(2\times2)$ twofold-site structure, formation of one domain would cause an asymmetry along the [110] and [1$\bar{1}$0] azimuths in terms of the Sn atom relative to the neighboring Ni atoms. In that case, which we can exclude, we would ob-

FIG. 4. Energy spectrum of 500-eV Li^+ scattered from a $c(2\times2)$-Sn/Ni(100) surface. The polar angle was 30°, and the laboratory scattering angle was 144°.
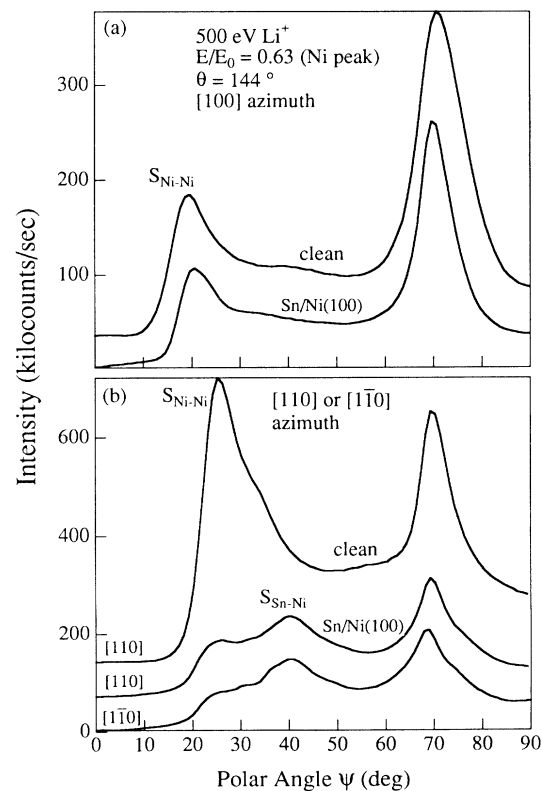

FIG. 5. Polar angle scans for 500 eV Li^+ ions scattered from Ni are compared for clean Ni(100) and $c(2\times2)$-Sn/Ni(100) along the [100] azimuth (a) and the [110] and [1$\bar{1}$0] azimuths (b).

serve an additional Sn shadowing Ni peak along either the [1$\bar{1}$0] or [110] azimuth, but not both. Since one expects an equal distribution of both possible domain orientations, lack of such asymmetry in our results is not a direct proof of the absence of the twofold-site structure. The most important evidence which excludes the twofold-site structure is that the Sn-Ni shadowing feature should appear well above 60° in the polar-angle scan if one assumes the Sn and Ni atoms retain their normal metallic radii. The Sn-Ni shadowing peak near 40° clearly excludes the model in which Sn adsorbs on twofold bridge sites. This conclusion is also supported by the observation of identical polar-angle scans for both azimuths. We are left with the surface-alloy model and, more specifically, a surface in which one-half monolayer of Sn atoms have substituted for the first-layer Ni atoms to form the $c(2\times2)$ structure. Based on this model, we expect that the polar-angle scan for the Ni-scattering intensity along the [100] azimuth will be the same for both clean Ni(100) and $c(2\times2)$-Sn/Ni(100), and that the polar scans along the [110] and [1$\bar{1}$0] azimuths will be equivalent. The agreement of the experimental results shown in Fig. 5 with these predictions strongly support the alloy model.

Although Sn atoms are incorporated into the first Ni layer, the $S_{\text{Sn-Ni}}$ peak in Fig. 5(b) indicates that the Sn atoms are not coplanar with neighboring Ni atoms, but buckled outward. This outward buckling produces the $S_{\text{Sn-Ni}}$ flux peak by Sn atoms shadowing the nearest-neighboring Ni atoms. The position of this peak is a sensitive function of the height of Sn above the first-layer Ni atoms, $d_{\perp}$, and can be used to determine that height. Based on the surface-alloy model, the predicted critical angle for the $S_{\text{Sn-Ni}}$ peak in the [110] azimuth is shown in Fig. 6 as a function of the buckling distance above the Ni
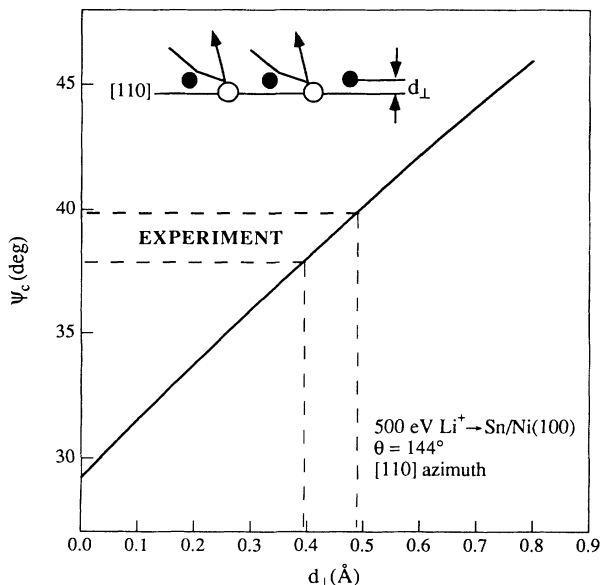
layer, along with the experimentally determined ψ_c value and associated error bars. The calculation was implemented using MARLOWE with a two-atom model. Based on multiple measurements, $\psi_c = 38.8\pm0.3°$ was obtained after sine correction of appropriate curves such as those in Fig. 5(b), and was chosen at 90% of the peak height after a background was subtracted from the $S_{\text{Sn-Ni}}$ peak. Since the value of ψ_c is affected by the background behavior, which is unknown to a certain extent, this causes an uncertainty in ψ_c. By trying different background curves, we estimate that at most a $\pm0.5°$ error can be introduced. The error in $d_\perp$ due to the uncertainty in the scattering potential should also be estimated. For a fairly large scattering angle, such as 144°, the predicated angle ψ_c is more sensitive to the potential of the shadowing atom than to the target atom, i.e., ψ_c is sensitive to the value of C for Li$^+$/Sn. An uncertainty of $\delta C_{\text{Sn}} = \pm0.03$ causes $\delta\psi_c = \pm0.6°$. If we also consider the polar-angle calibration uncertainty which is $<0.5°$, the total uncertainty should be $\delta\psi_c < 1.0°$. This results in our determination of $\psi_c = 38.8\pm1°$ at a high level of confidence. From the above consideration of the errors in the measurements, the buckling distance $d_\perp$ is determined to be 0.44 ± 0.05 Å.

Structural information can also be obtained from the polar-angle dependence of the Sn single scattering curves shown in Fig. 7. If there were subsurface (second or third layer) Sn atoms, we would have seen additional features at high polar angles. Only one shadowing peak $S_{\text{Sn-Sn}}$ at a low polar angle and the flat angular dependence above 30° indicate that Sn is in the topmost layer of the surface. Thus all of the experimental evidence is consistent and confirms that the $c(2\times2)$-Sn/Ni(100) structure is due to a surface-alloy phase with Sn protruding slightly (0.44 Å) above the first Ni layer.
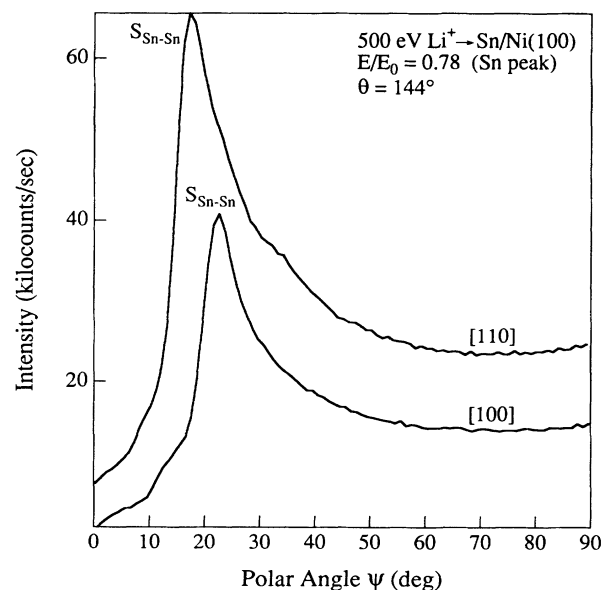

FIG. 6. The calculated critical angle ψ_c of the $S_{\text{Sn-Ni}}$ peak along the [110] azimuth is shown as a function of the perpendicular height of the Sn atoms above the first Ni layer. The experimentally measured critical angle is denoted by the dashed lines.

FIG. 7. Polar-angle scans of 500-eV Li$^+$ ions scattered from Sn for the $c(2\times2)$-Sn/Ni(100) surface along both [110] and [100] azimuths.

D. Structure changes induced by annealing

It is apparent from Sec. III C that Sn atoms are inter-mixed with Ni atoms even at a deposition temperature of 250 K. Annealing this surface presumably forms a more highly ordered and stable bimetallic surface. Experimentally we see that the $c(2 \times 2)$ LEED pattern persists upon annealing to 800 K, and the sharpest pattern occurs after annealing to 600–800 K. On the other hand, additional features were observed in the polar-angle scans once the surface was annealed to 400 K, and these features remained constant until 800 K. Once the surface was annealed to 900 K, a complex LEED pattern appeared, and further changes in the polar-angle scans were observed. Figure 8 displays the results for Sn and Ni polar scans along different azimuths at 250 K (the Sn deposition temperature) and two subsequent annealing temperatures of 600 and 900 K.

We first examine the spectra at 600 K. In the [110] direction, the polar-angle scans retained the old features, but some slight shifts in the peak positions were observed. The S_{Sn-Ni} peak in Fig. 8(a) shifts to a larger polar angle by 2°, but the peak width and shape are almost the same as those before annealing. The S_{Sn-Sn} peak in Fig. 8(b) also shifts up by 2°. In the [100] direction, the S_{Sn-Sn} peak in Fig. 8(d) remains the same, but dramatic
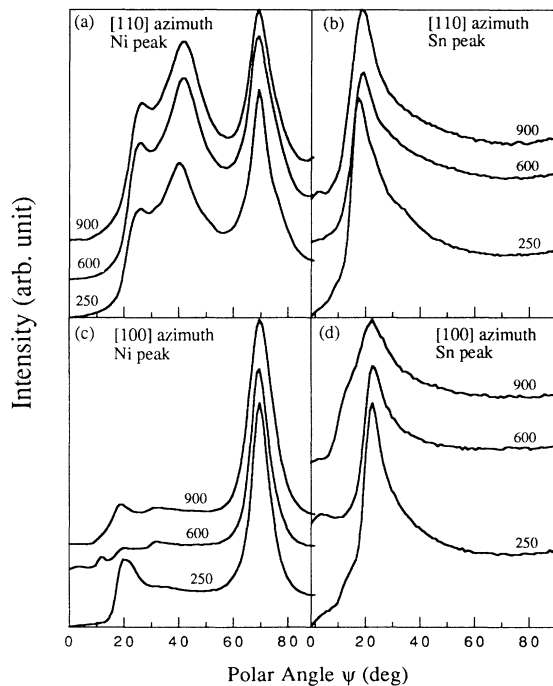

FIG. 8. Polar-angle scans of 500-eV Li^+ scattering from Sn/Li(100) surfaces following deposition at 250 K, and after brief annealing to 600 and 900 K, respectively. The Sn/Ni(100) surfaces formed at 250 and 600 K showed a $c(2 \times 2)$ LEED pattern, and a complex LEED pattern was formed after annealing to 900 K. (a) $Li^+ \rightarrow Ni$ single scattering along [110] azimuth. (b) $Li^+ \rightarrow Sn$ single scattering along [110]. (c) $Li^+ \rightarrow Ni$ single scattering along [100]. (d) $Li^+ \rightarrow Sn$ single scattering along [100].

changes are found for the $Li^+ \rightarrow Ni$ single scattering features. As shown in Fig. 8(c), the S_{Ni-Ni} peak is split upon annealing into three weak, separated peaks. It is difficult to reconcile these changes along the [100] azimuth with the almost unaltered curves along the [110] azimuth. Since all of these changes are observed at small incidence angles, they are related to surface lattice distortions on the outermost layer of the Sn/Ni(100) surface. We believe that the main features of the $c(2 \times 2)$ structure are unchanged after annealing for two reasons. First, the $c(2 \times 2)$ LEED pattern persists during the annealing process; no new features appear and the $c(2 \times 2)$ pattern becomes sharper when the surface is annealed to 600 K. Second, the main features of the polar-angle scans are retained after annealing, therefore the overlayer models proposed in Fig. 3 are still inapplicable. This suggests that the annealed Sn/Ni(100) surface has a similar alloy structure to the one we described in Sec. III C. The splitting of the S_{Ni-Ni} peak along the [100] azimuth could be the result of small amplitude periodic distortions of Ni atoms in the first layer. We are currently unable to propose explicitly a reconstructed surface model which can account all of the features that appeared in our polar-angle scans after annealing.

Although the cold-deposited Sn/Ni(100)-$c(2 \times 2)$ surface alloy maintains a constant surface structure up to 400 K, the polar-angle scans of the $c(2 \times 2)$ structure formed by depositing 0.5-ML Sn at 330–340 K resemble those obtained after annealing the cold-deposited sample to above 400 K, i.e., we clearly see the splittings of the S_{Ni-Ni} peak along the [100] azimuth. This suggests that the Sn deposition temperature has to be much lower than 400 K in order to obtain the alloyed surface described in Sec. III C.

After annealing the alloyed surface to 900 K, a LEED pattern was observed that was characterized by a splitting of each half-integer beam spot into a quartet. A Sn coverage of ≈ 0.4 ML was determined from AES for this pattern. A similar LEED pattern has been observed in the case of nitrogen adsorption on W(100),[14] where the splitting of each half-order spot into a quartet occurs at a N coverage of $0.3 \leq \theta_N \leq 0.4$. This structure was attributed to the formation of out-of-phase islands, which consist of nitrogen adatoms in a (4×4) structure. Based on intensity asymmetry within the half-order quartet, Griffiths and King[15] further proposed the "contracted domain" idea, in which the four tungsten atoms adjacent to the N adatom were all uniformly displaced toward the N adatom. We did not observe any obvious intensity modulation within the quartets for Sn/Ni(100), but this was not studied in any detail. Even if there is a contraction within the domain, it is fairly small in our case since our overall angular scans still retain the original main features. Similarly to N/W(100), we can also estimate the domain size from the Sn coverage of $\theta_{Sn} \approx 0.4$ ML to be about 16 Sn atoms. Figure 8 shows that the polar-angle scans after annealing to 900 K are almost indistinguishable from those at 600 K in the [110] direction, except the S_{Sn-Ni} and S_{Sn-Sn} peaks are shifted back by about 1° to lower polar angles. Striking differences are seen in Fig. 8(c) in the $Li^+ \rightarrow Ni$ polar-angle scan along the [100] az-

imuth for the surface annealed to 900 K compared to that annealed to 600 K. The first peak is no longer observable, and is replaced by a broad shoulder, and the peak at 20° is greatly enhanced. These changes make the overall $Li^+ \rightarrow Ni$ polar-angle scan along the [100] azimuth look more like the one for the cold-deposited surface without annealing. In the corresponding $Li^+ \rightarrow Sn$ polar scan at 900 K seen in Fig. 8(d), an additional shoulder appears around 10°, which indicates that a different Sn-Sn distance might be formed within the alloyed layer. The surface seems to have undergone another reconstruction which produces local geometric structures similar to those at a deposition temperature of 250 K.

E. Depth distribution of Sn atoms

To demonstrate clearly the surface-alloy nature of Sn on Ni(100), we studied the depth profile of Sn atoms in the Ni-substrate when excess Sn was deposited initially. No LEED pattern was observed after about 0.8 ML of Sn was deposited at 250 K. After the sample was flashed to 700 and 900 K, clear and sharp $c(2\times2)$ LEED patterns were observed at both temperatures (in Sec. III D, we described how annealing to 900 K for an initial Sn coverage of 0.5 ML resulted in a complex LEED pattern). Figure 9 shows the polar-angle scan of Sn single scattering along the [100] azimuth for these two annealing temperatures. The peak at about 70°, which is related to subsurface Sn, can be seen clearly at 700 K, but is absent at 900 K. Although the depth profile of Sn is unknown, certainly any excess Sn that is dissolved into the bulk is not present in the second and third layers once the sample is annealed to 900 K. This result demonstrates that the $c(2\times2)$
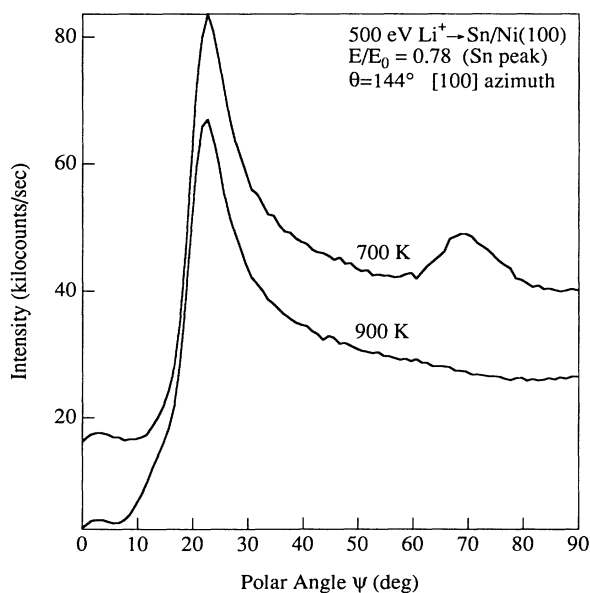

FIG. 9. Polar-angle scans of $Li \rightarrow Sn$ single scattering along the [100] azimuth are shown after annealing the Sn/Ni(100) surface to 700 and 900 K. A $c(2\times2)$ LEED pattern was formed at both temperatures. Sn was deposited at 250 K with an initial coverage of $\theta_{Sn}=0.9$ ML, and no LEED pattern was observed at this temperature.

structure is a truly two-dimensional phase. The depth distribution of Sn in Ni is temperature sensitive and coverage dependent. Annealing to high temperatures can help to reduce the amount of Sn trapped in the near-surface region when excessive amounts of Sn are deposited initially on the surface. Similar results were found by Ku and Overbury.[8] When excess Sn was deposited on Ni(111), they found that an additional peak appeared in the Sn incident-angle dependence scans. When the sample was flashed to 1000 K, this subsurface Sn peak decreased but was never totally eliminated.

IV. DISCUSSION

The formation of an ordered surface alloy of Sn on the Ni(100) surface is due mainly to the much lower surface free energy of Sn (541 $erg\,cm^{-2}$) vs Ni (1706 $erg\,cm^{-2}$), the exothermic heat of formation of Sn-Ni alloys (about 5.6 kcal/mole for Ni_3Sn),[17] and the strongly ordered intermetallic phases of $Ni_{1-x}Sn_x$. The high solubility of Sn in Ni also facilitates the process of dissolving excess Sn into the Ni substrate, producing a true Sn/Ni(100) surface-alloy phase. It is interesting to note that the reaction of Al atoms with a Ni(100) surface does not seem to produce a surface alloy. Lu et al.[18] report that annealing Al films (1–2 ML) to 850 K leads to well-crystallized epitaxial films of $Ni_3Al(100)$, indicating that the mixing of Al atoms with the substate Ni atoms penetrates deeper than the first layer of the substrate. This behavior is suggested by these authors to be due to the very close match (1%) of the Ni lattice spacing to that of Ni_3Al after comparing with the $c(2\times2)$-Au/Cu(100) surface-alloy system,[3] which has a 4% mismatch between Cu and Cu_3Au. In our Sn/Ni(100) case, the lattice mismatch of Ni to Ni_3Sn is 6%. Therefore, this kind of size mismatch might be necessary for surface-alloy formation.

There are several ways to prepare the $c(2\times2)$-Sn/Ni(100) surface alloy. One approach is to deposit the right amount of Sn (0.5 ML) on the Ni(100) surface, and this can be done over quite a wide range of temperatures. The other way is to put an excess of Sn on the surface and then anneal the surface to higher temperatures (600–900 K, depending on the initial coverage). It is important to realize that the resulting alloyed surfaces are not identical from these two approaches. As pointed out in Sec. III D, the Sn/Ni(100)-$c(2\times2)$ alloyed surfaces formed by depositing Sn at 250 K and by annealing the surface to above 400 K have different angle-dependent features (Fig. 8). Annealing may facilitate additional, although small, surface reconstruction. We also noticed that the $c(2\times2)$ LEED pattern was sharpened once the sample was annealed to elevated temperatures, indicating the formation of a highly ordered alloy surface. This observation suggests that the Sn/Ni(100) surface prepared at 250 K is not fully ordered, and a small fraction of Sn may not be in the $c(2\times2)$ structure. Figure 7 shows that these disordered Sn atoms do not reside above or below the mixed layer within the experimental sensitivity of ≤ 0.03 ML, since no additional peak was found at higher incident angles. Possible locations of the disordered Sn atoms are at the boundaries of domains that might be

formed when Sn is deposited at 250 K. Annealing to 600 K increases the domain size, giving a more nearly perfect $c(2\times2)$ structure. This hypothesis also helps us to understand the differences in the Ni incidence angle scans at 250 and 600 K shown in Fig. 8(c). The incorporation of Sn atoms into the first Ni layer certainly introduces a large strain into the lattice, which is released partially by Sn atoms protruding above the first Ni layer. The rest of the strain needs to be released by another channel. Small amplitude periodic distortions within the large domains themselves may release the additional strain for the perfect $c(2\times2)$ structure formed by annealing to 600 K, which leads to the splitting of the S_{Sn-Sn} peak observed in Fig. 8(c). On the other hand, if the $c(2\times2)$ structure consists of relatively small domains, this additional strain can be released through the domain boundaries, and then we should have an undistorted $c(2\times2)$ structure inside the domains. This might be why we did not see the peak splitting in the Ni polar-angle scans at 250 and 900 K in Fig. 8(c). Additional experiments, e.g., utilizing scanning-tunneling microscopy (STM) or other techniques, are needed to resolve these issues.

Sn deposition has been studied systematically on the (111) surfaces of Cu, Ni, and Pt by Overbury and Ku[7] using ALISS. Stable and ordered two-dimensional surface alloys are formed on all three substrates upon annealing to 600–1000 K. They also found that Sn atoms were not coplanar with the first-layer substrate atoms, and the amount of outward buckling was linearly correlated to the lattice constant of the substrates. The buckling for $p(\sqrt{3}\times\sqrt{3})$-Sn/Ni(111) is $d_\perp=0.46\pm0.04$ Å, which is almost identical to our $c(2\times2)$-Sn/Ni(100) result of 0.44 ± 0.05 Å. The value of $d_\perp$ is related directly to the bond distance between the Sn atom and first-layer Ni atoms, but it is not clear yet what determines this bond distance. Two possible mechanisms have been suggested. One is based on the strain relief associated with incorporation of the larger Sn atoms into the Ni lattice, i.e., size mismatch. The other is based on the surface relaxation associated with charge-transfer and electrostatic neutrality.[19] The same amount of buckling observed for Sn on Ni(111) and (100) faces indicates that buckling does not depend upon first- and second-layer coordinations, specially for Sn/Ni alloys. This fact also constrains possible theories for the mechanism of surface rippling.

V. CONCLUSIONS

Sn mixes with Ni(100), forming an ordered $c(2\times2)$ two-dimensional surface alloy with Sn rippling above the first Ni layer by 0.44 ± 0.05 Å. This ordered alloy surface can even be formed at 250 K, showing that mixing of Sn and Ni occurs at low temperatures. Annealing this $c(2\times2)$ alloy surface with $\theta_{Sn}=0.5$ ML formed at 250 K to above 400 K, but less than 800 K, introduces further surface reconstruction, possibly as small amplitude periodic distortions within the mixed layer. Annealing to above 900 K produces a complex LEED pattern that is explained based on domain formation. This surface alloy of $c(2\times2)-$Sn/Ni(100) is a truly two-dimensional phase, since virtually no Sn atoms can be found in the second or third layers below the surface. Finally, the similarity in the amount of buckling in the surface alloy formed for Sn/Ni(100) and Sn/Ni(111) shows that buckling does not depend on first- and second-layer coordination of Sn and Ni.

ACKNOWLEDGMENTS

[1]*Physical and Chemical Properties of Thin Metal Overlayers and Alloy Surfaces*, edited by D. M. Zehner and D. W. Goodman (Materials Research Society, Pittsburgh, 1987).

[2]C. T. Campbell, Ann. Rev. Phys. Chem. **41**, 775 (1990).

[3]Z. Q. Wang, Y. S. Li, C. K. Lok, J. Quinn, F. Jona, and M. Marcus, Solid State Commun. **62**, 62 (1987).

[4]S. C. Wu, S. H. Lu, Z. Q. Wang, C. K. C. Lok, J. Quinn, Y. S. Li, D. Tian, and F. Jona, Phys. Rev. B **38**, 5363 (1988).

[5]M. T. Paffett and R. G. Windham, Surf. Sci. **208**, 34 (1989).

[6]S. H. Overbury, D. R. Mullins, M. F. Paffett, and B. E. Koel, Surf. Sci. **254**, 45 (1991).

[7]S. H. Overbury and Yi-sha Ku, Phys. Rev. B **46**, 7868 (1992).

[8]Yi-sha Ku and S. H. Overbury, Surf. Sci. **273**, 353 (1992).

[9]M. T. Paffett, S. C. Gebhard, R. G. Windham, and B. E. Koel, Surf. Sci. **223**, 449 (1989).

[10]M. T. Paffett, S. C. Gebhard, R. G. Windham, and B. E. Koel, J. Phys. Chem. **94**, 6831 (1990).

[11]M. T. Paffett, A. D. Logan, R. J. Simonson, and B. E. Koel, Surf. Sci. **250**, 123 (1991).

[12]O. Oda and G. E. Rhead, Surf. Sci. **92**, 467 (1980).

[13]L. Q. Jiang, Y. D. Li, and B. E. Koel, Phys. Rev. Lett. **70**, 2649 (1993).

[14]D. L. Adams and L. H. Germer, Surf. Sci. **26**, 109 (1971).

[15]K. Griffiths, C. Kendon, and D. A. King, Phys. Rev. Lett. **46**, 1584 (1981).

[16]S. H. Overbury and D. R. Huntley, Phys. Rev. B **32**, 6278 (1985).

[17]R. Hultgren, R. L. Orr, P. D. Anderson, and K. K. Kelley, *Selected Values of Thermodynamic Properties of Metals and Alloys* (Wiley, New York, 1963).

[18]S. H. Lu, D. Tian, Z. Q. Wang, T. S. Li, and F. Jona, Solid State Commun. **67**, 325 (1988).

[19]J. I. Lee, C. L. Fu, and A. J. Freeman, Phys. Rev. B **36**, 9318 (1987).